USGS
science for a changing world

Mapping with Imaging Spectroscopy, Fort Cobb Reservoir Watershed, Southwestern Oklahoma

Chapter 6 of

Assessment of Conservation Practices in the Fort Cobb Reservoir Watershed, Southwestern Oklahoma

Compiled by the U.S. Geological Survey and the Agricultural Research Service

Scientific Investigations Report 2010–5257

U.S. Department of the Interior
U.S. Geological Survey

Mapping with Imaging Spectroscopy, Fort Cobb Reservoir Watershed, Southwestern Oklahoma

By Roger N. Clark and Richard A. Wise

Chapter 6 of
Assessment of Conservation Practices in the Fort Cobb Reservoir Watershed, Southwestern Oklahoma

Compiled by the U.S. Geological Survey and the Agricultural Research Service

Scientific Investigations Report 2010–5257

U.S. Department of the Interior
U.S. Geological Survey

U.S. Department of the Interior
KEN SALAZAR, Secretary

U.S. Geological Survey
Marcia K. McNutt, Director

U.S. Geological Survey, Reston, Virginia: 2011

This and other USGS information products are available at http://store.usgs.gov/
U.S. Geological Survey
Box 25286, Denver Federal Center
Denver, CO 80225

To learn about the USGS and its information products visit http://www.usgs.gov/
1-888-ASK-USGS

Suggested citation:
Clark, R.N., and Wise, R.A., 2011, Mapping with imaging spectroscopy, Fort Cobb Reservoir watershed, southwestern Oklahoma, chap. 6 *of* Becker, C.J., ed., Assessment of conservation practices in the Fort Cobb Reservoir watershed, southwestern Oklahoma: U.S. Geological Survey Scientific Investigations Report 2010–5257, 23 p.

Contents

Figures

Tables

Conversion Factors

SI to Inch/Pound

Multiply	By	To obtain
	Area	
square meter (m^2)	0.0002421	acre
square kilometer (km^2)	247.1	acre
square kilometer (km^2)	0.3861	square kilometer (km^2)
	Length	
meter (m)	3.281	foot (ft)
kilometer (km)	0.6214	mile (mi)

Vertical and horizontal coordinate information is referenced to the World Geodetic System of 1984 (WGS84).

Elevation, as used in this report, refers to distance above the vertical datum.

Mapping with Imaging Spectroscopy, Fort Cobb Reservoir Watershed, Southwestern Oklahoma

By Roger N. Clark and Richard A. Wise

Abstract

Imaging spectroscopy was used to estimate concentrations of selected compounds in the Fort Cobb Reservoir watershed to investigate conditions affecting water quality in the Fort Cobb Reservoir. The satellite-based Hyperion imaging spectrometer was used because of low cost and data availability. The data were acquired in September and October 2006. A portable field spectrometer was used in September 2006 to measure characteristic spectral reflectance properties of soils in the region. The data from the field spectrometer were used to calibrate the Hyperion data, removing atmospheric scattering and absorptions and removing the solar spectrum, resulting in calibrated reflectance spectra on a 30-meter spatial grid throughout the imaged area. The spectra were then analyzed to search for compounds in each spectrum and maps of various compounds were made. Chlorophyll in water produces a characteristic peak in reflectance near 0.6 microns. Maps of the strength of the chlorophyll in the Fort Cobb Reservoir indicated that multiple sources of nutrients may be causing areas of increased chlorophyll concentrations. Major streams make some contribution to the chlorophyll; however, minor streams draining directly from cultivated fields appear to contribute greater proportions of the chlorophyll plumes in the reservoir than larger creeks, which are buffered by natural ecosystems. These results indicated that increasing the area of natural ecosystems of minor and major drainages may help mitigate nonpoint source pollution from farming practices in the watershed.

Iron oxide spectral abundance was greatest in bare farm fields, with a tendency for stronger spectral signatures to the north. This strong spectral signature corresponded to the reddish coloration of the soils during field calibration efforts. Local crops and/or farming practices might preferentially leach iron oxide from the soil, thus explaining why some fields had different iron oxide spectral strengths compared to adjacent fields.

The terrestrial vegetation spectral map indicated no obvious trend in relation to chlorophyll abundance in the reservoir. Confounding investigation of a possible relation between these features is the fact that line FCRW2 was obtained nearly a month after line FCRW1 and terrestrial vegetation was senescing with the start of autumn.

Introduction

In this chapter, data from the satellite-based Hyperion imaging spectrometer (Pearlman and others, 2001) and field sampling were used to estimate concentrations of selected compounds in the Fort Cobb Reservoir watershed as part of a larger study, conducted in cooperation with the Agricultural Research Service of the U.S. Department of Agriculture and the U.S. Geological Survey to use multiple lines of evidence to investigate hydrologic, geologic, and geographic features which may affect eutrophication of a reservoir in a rural watershed, and to better determine sources of sediments and associated nutrients to the reservoir.

Spectroscopy

Spectroscopy is a tool that has been used for decades to identify, understand, and quantify solid, liquid, or gaseous compounds, commonly in the laboratory. In disciplines ranging from astronomy to chemistry, spectroscopic measurements are used to detect absorption features caused by specific chemical bonds, with the analyses being used to determine the abundance and physical state of the detected absorbing species. Imaging spectroscopy is a tool that can be used to spectrally identify and spatially map compounds having specific chemical bonds (Clark and others, 2003a).

Geology of the Fort Cobb Reservoir Watershed

The Fort Cobb Reservoir is a 16.6-square-kilometer reservoir in Caddo County, in the Anadarko Basin of southwestern Oklahoma. The reservoir lies in an 813-square-kilometer watershed (fig. 1) characterized by predominantly sandy loam soils. During the middle of the Pennsylvanian Period, a great amount of sediments were deposited in the Anadarko Basin. That deposition was followed by a transgression of the sea into the basin during the Permian Period. Marine rocks were deposited into that shallow sea, including evaporates such as anhydrite, gypsum, and halite, and some shale and dolomite (Suneson and Johnson, 1996).

The Fort Cobb Reservoir watershed includes three subwatersheds: Cobb Creek (includes the Fivemile Creek subwatershed), Lake Creek, and Willow Creek (see chapter 3, fig. 1, this volume). Permian-age rocks and soils developed on those rocks are commonly visible in the Cobb Creek subwatershed. In this system, the Whitehorse Group, consisting of the Rush Springs Sandstone and Marlow Formation, is the main unit. The Marlow Formation consists of massive gypsum units, interbedded sandstones, siltstones, mudstones, gypsum-anhydrite, and dolomite beds. Overlying the Marlow Formation, the Rush Springs Sandstone consists of cross-bedded sandstone with interbedded dolomite and gypsum. The Rush Springs Sandstone is reddish brown to orange brown in color, the color resulting from a thin coat of oxidized iron minerals on clastic sediment particles (Suneson and Johnson, 1996).

Soils throughout Caddo County are formed mainly from regolith derived from the Rush Springs Sandstone—the sandstone, shale, limestone, gypsum, and Quaternary-age alluvium and terrace deposits (Runkle and others, 1997).

Purpose and Scope

The purpose of this chapter is to use a synoptic view of imaging spectroscopy remote sensing to map selected compounds in the Fort Cobb Reservoir watershed to provide information about sources of compounds that may be affecting water quality in the watershed. An advantage of imaging spectroscopic remote sensing is that it provides continuous synoptic sampling over large areas with tens-of-thousands of samples (pixels in an image). Disadvantages of this method include: (1) only the optical surface is probed (and, therefore, rocks and soils can be hidden by overlaying vegetation); and (2) limited sensor spectral range, spectral resolution, signal-to-noise ratio, and atmospheric absorptions reduce detection to less than what can be achieved by laboratory analyses. However, limited field sampling efforts do not collect as many samples for analyses as remote sensing can, thus field sampling may miss major potential sources of sediments and nutrients. Therefore, remote sensing provides a complimentary dataset to field water-quality sampling for analyzing selected characteristics of large regions.

For this chapter, an experimental sensor, the Hyperion Imaging Spectrometer (Pearlman and others, 2001) was the only available sensor that could provide the required remote sensing data within available project resources. The Hyperion sensor measures spectra from the ultraviolet (0.35 microns) to the near-infrared (2.5 microns). The signal-to-noise ratio was not as high as other sensors, but the signal-to-noise ratio of the Hyperion sensor is adequate for compounds with major absorption bands in the spectra. Six satellite passes from September 9, 2006, to October 24, 2006, were required to cover the watershed (fig. 2, table 1). Because of limited project resources, only the lines FCRW1 and FCRW2 that cover the Fort Cobb Reservoir were calibrated and analyzed for this report (fig. 2).

Methods

Data Calibration

The Hyperion data were calibrated by using the radiative transfer-ground calibration method described in Clark and others (2002). This method uses a radiative transfer model to compute and remove absorptions caused by atmospheric gases, including water vapor, oxygen, carbon dioxide, methane, and ozone. The solar spectrum was removed and the scattering caused by aerosols was approximated and removed.

Field locations were characterized by collecting samples along public roadways where soils visually matched adjacent bare fields. The sample locations are listed in table 2 and shown in figure 3, with spectra being shown in figures 4*A*-4*H*. Representative spectra in the Hyperion dataset were extracted in the regions of each sample location and compared with the in situ spectra, obtained from the field samples. A portable field spectrometer was used in September 2006 to measure characteristic spectral reflectance properties of soils in the region and an asphalt parking lot referred to as calibration site C1 (table 2). The data from the field spectrometer were used to calibrate the Hyperion data, removing atmospheric scattering and absorptions and removing the solar spectrum, resulting in calibrated reflectance spectra on a 30-meter spatial grid throughout the imaged area. The image data spectra were then analyzed to search for compounds in each spectrum and maps of various compounds were constructed. The radiative transfer models are imperfect and the in situ spectra were used to correct the residuals (Clark and others, 2002). Unfortunately, the Hyperion sensor contains residual noise sources that limited compositional results compared to what might be possible with higher precision sensors such as AVIRIS (Clark and others, 2003a).

Hyperion line FCRW2 had anomalous behavior compared to line FCRW1. An offset appeared in the visible part of the spectrum in some channels that prevented mapping of vegetation and iron oxides. A custom software algorithm

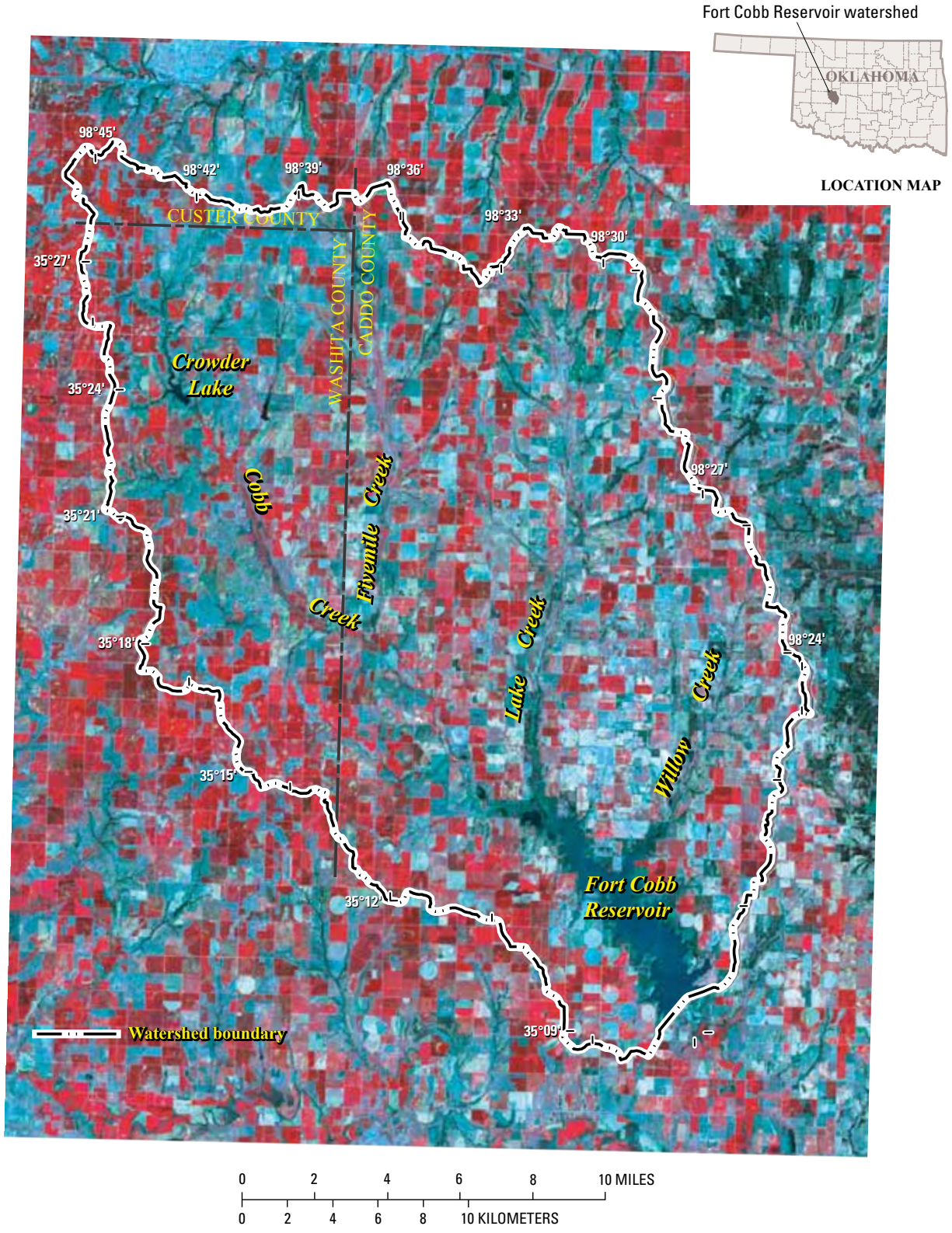

Figure 1. The Fort Cobb Reservoir watershed, southwestern Oklahoma, shown on an ASTER (Advanced Spaceborne Thermal Emission and Reflection Radiometer) band 1, 2, 3 (blue, green, red) color composite image. (Cultivated fields are readily identified by the shape (circle or square). Bare soil appears as shades of cyan and dense green vegetation as red. Natural areas around streams and lakes tend to appear as blue-green.)

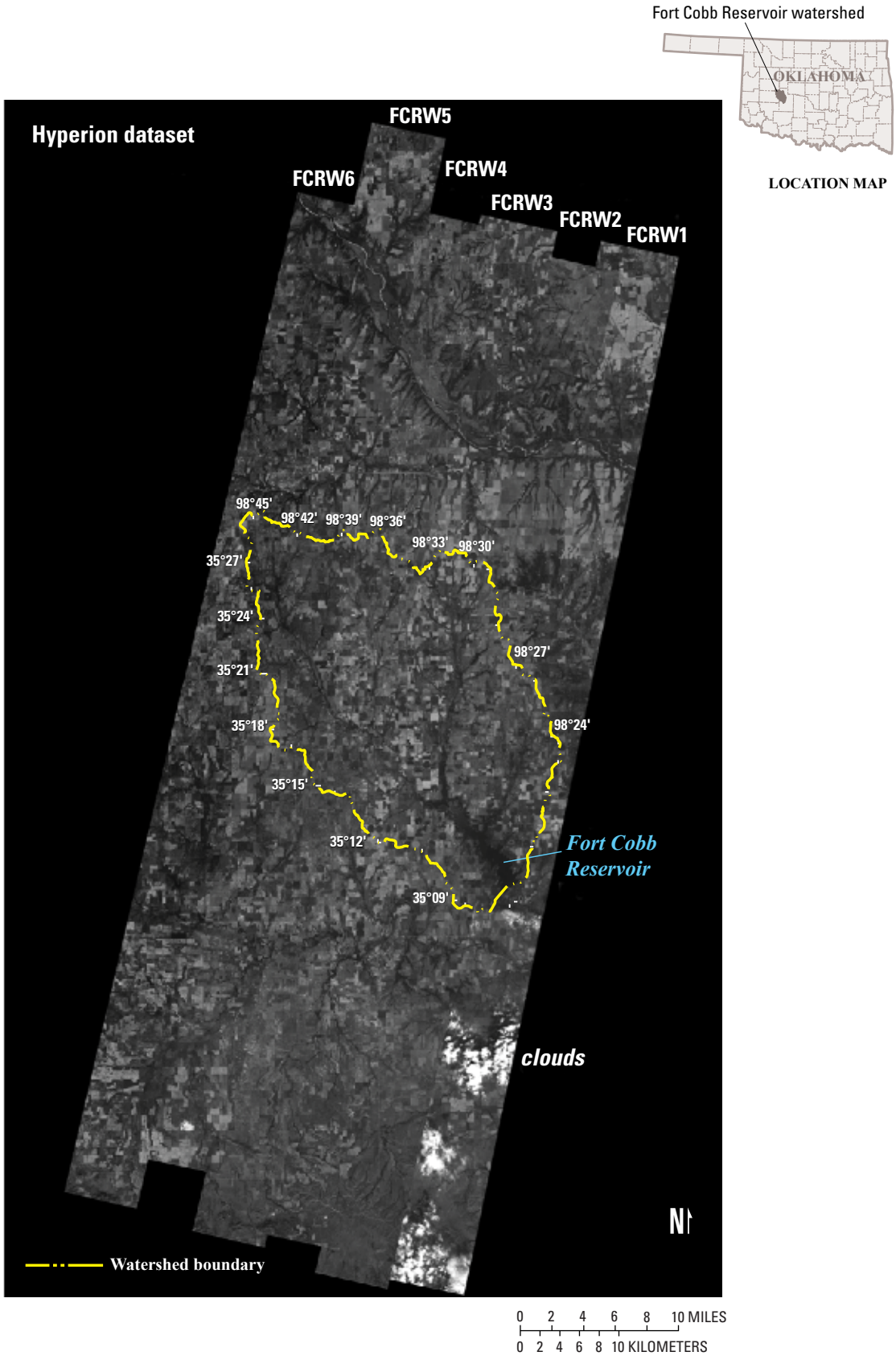

Figure 2. Image showing six Hyperion flight lines of the Fort Cobb Reservoir watershed, southwestern Oklahoma, 2006. (See table 1 for dates and times of data acquisition.)

Table 1. Dates and times of Hyperion data collection for the FCRW1 and FCRW2 flight lines for the Fort Cobb Reservoir, southwestern Oklahoma, 2006.

[yyyy/mm/dd, year/month/day; GMT, Greenwich Mean Time]

Flight line	Date of acquisition (yyyy/mm/dd)	Start time of line (GMT)
FCRW1	2006/09/09	16:51:43
FCRW2	2006/10/14	16:59:15
FCRW3	2006/09/19	16:53:53
FCRW4	2006/10/19	17:00:19
FCRW5	2006/09/29	16:56:02
FCRW6	2006/10/24	17:01:21

Table 2. Location and sample information for field samples collected for calibrating the Hyperion data in the Fort Cobb Reservoir watershed, southwestern Oklahoma, 2006.

[ID, identifier; °, degrees; ‘, seconds: N, north:W, west; CR, county road]

Sample ID	Latitude [1]	Longitude [1]	Elevation (feet) [1]	Sample information
ftc06-C1	35°11.85’N	98°28.62’W	1,330	Asphalt parking lot: calibration site C1, same location on figure 3 as ftc06-05
ftc06-01	35°19.104’N	98°39.522’W	1,469	Soil sample collected along road
ftc06-02	35°10.663’N	98°25.495’W	1,371	Soil sample from road cut near Fort Cobb State Park 0.2 mile north of CR E1270 and CR N2570
ftc06-03	35°10.586’N	98°27.057’W	1,376	Sandstone sample 200 feet west of ftc06-02 location
ftc06-04	35°10.583’N	98°27.057’W	1,378	Soil sample
ftc06-05	35°11.85’N	98°28.623’W	1,330	Sandstone sample by calibration site C1
ftc06-06	35°14.750’N	98°31.069’W	1,419	Soil sample 0.1 mile southeast of intersection CR E1270 and CR S2510
ftc06-07	35°14.750’N	98°31.059’W	1,419	Soil sample 0.1 mile southwest of intersection CR E1270 and CR S2510
ftc06-08	35°10.516’N	98°26.067’W	1,377	Gravel road intersection on CR E1270 and farm access road, just outside of Fort Cobb State Park headquarters.
ftc06-09	35°10.516’N	98°26.067’W	1,377	Same as above with larger rocks
ftc06-10	35°11.790’N	98°25.448’W	1,442	Soil sample from dirt field on right side State Highway 146 and north of CR E1260
ftc06-11	35°17.432’N	98°31.060’W	1,463	Soil sample just southeast of intersection CR S2510 and State Highway152
ftc06-12	35°17.460’N	98°34.223’W	1,450	Gravel sample at Hoochie Mamas Restaurant gravel parking lot State Highways 152 and 58
ftc06-13	35°18.020’N	98°34.238’W	1,497	Soil sample at State Highway 58 north of State Highway 152
ftc06-14	35°24.376’N	98°35.274’W	1,579	Soil sample southeast of intersection CR Ell10 and CR S2470
ftc06-15	35°24.376’N	98°35.274’W	1,579	Soil sample northeast of intersection CR Ell10 and CR S2470
ftc06-16	35°24.322’N	98°41.786’W	1,578	Soil sample just north of entrance to Crowder Lake State Park
ftc06-17	35°24.322’N	98°41.788’W	1,578	Soil sample at same location as ftc06-16

[1] Datum is the World Geodetic System of 1984.

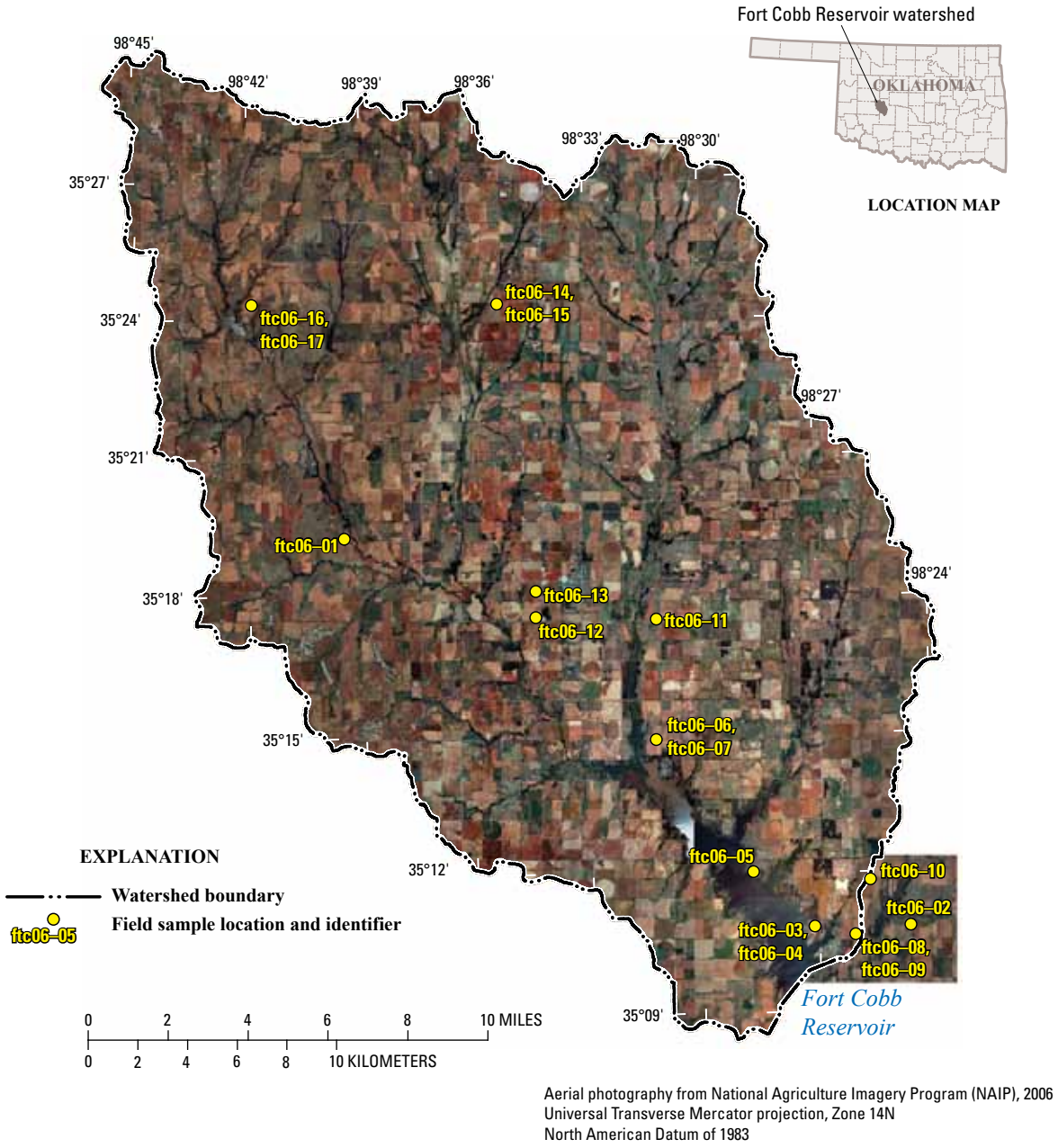

Figure 3. Locations where field samples were collected for calibrating the Hyperion data in the Fort Cobb Reservoir watershed, southwestern Oklahoma, 2006.

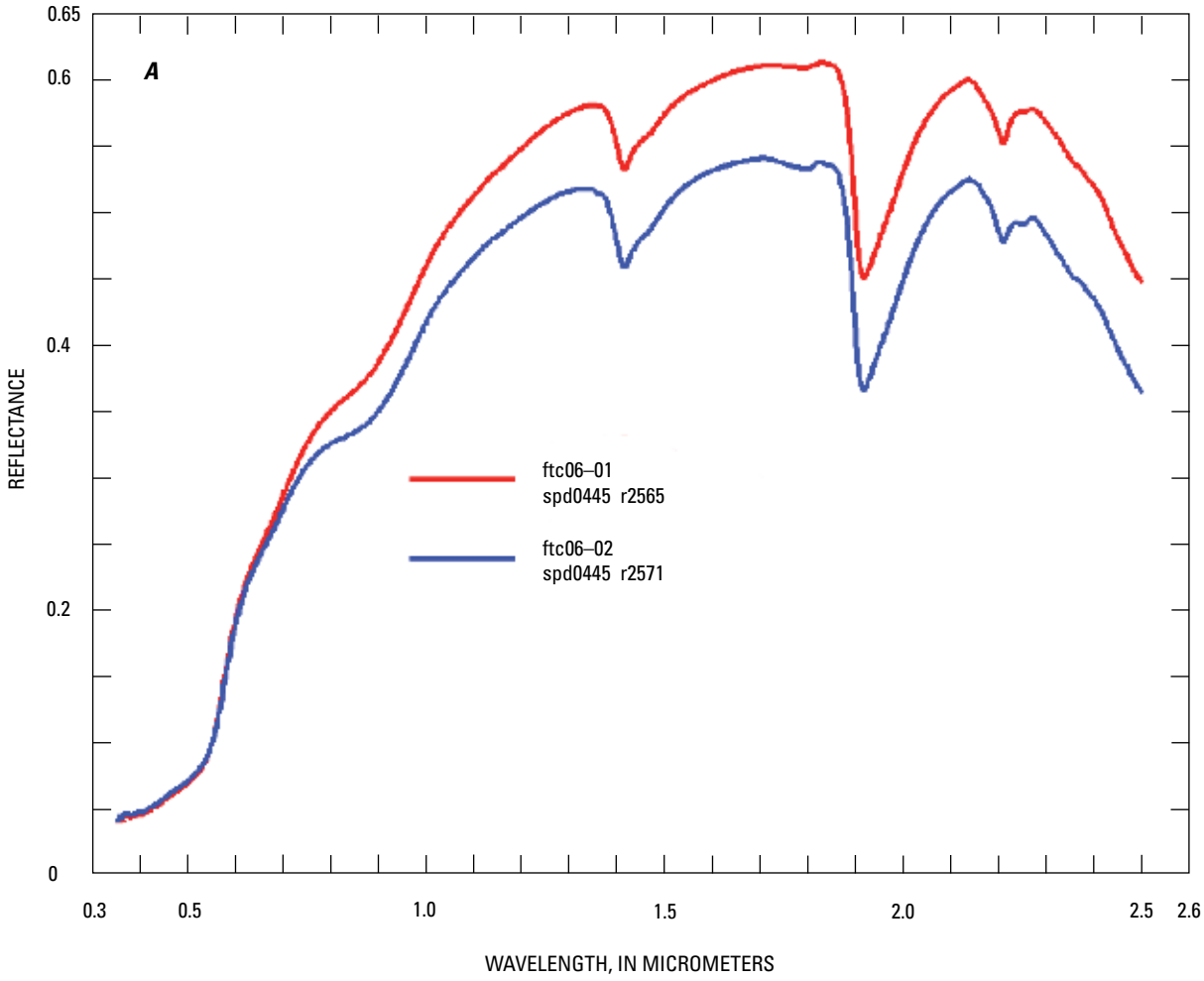

Note:
spd, spectral power distribution of the illuminant
r, reflectance of the object

Figure 4. Spectra obtained in the field for samples from Fort Cobb Reservoir watershed, southwestern Oklahoma. *A*, ftc06–01 and ftc06–02. *B*, ftc06–C1. *C*, ftc06–03 and ftc06–04. *D*, ftc06–05, ftc06–06, ftc06–10, and ftc06–11. *E*, ftc06–07 (high water content compared to ftc06–10 and ftc06–11. *F*, carbonate (dolomite) road gravel ftc06–08, ftc06–09, and ftc06–12. *G*, ftc06–13, ftc06–14, and ftc06–15. *H*, Flowers surrounding the C1 calibration site.

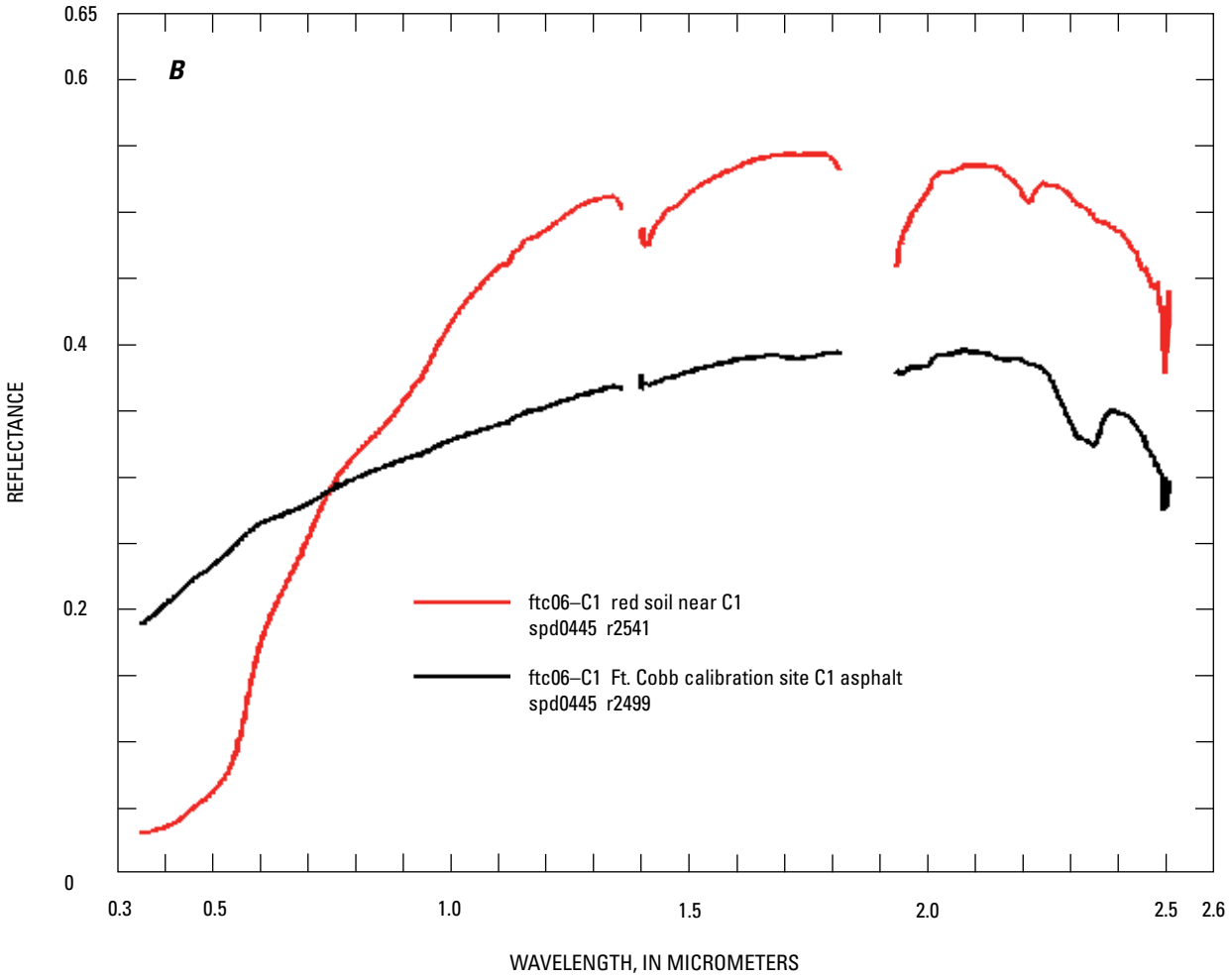

Note:
spd, spectral power distribution of the illuminant
r, reflectance of the object

Figure 4. Spectra obtained in the field for samples from Fort Cobb Reservoir watershed, southwestern Oklahoma. *A*, ftc06–01 and ftc06–02. *B*, ftc06–C1. *C*, ftc06–03 and ftc06–04. *D*, ftc06–05, ftc06–06, ftc06–10, and ftc06–11. *E*, ftc06–07 (high water content compared to ftc06–10 and ftc06–11. *F*, carbonate (dolomite) road gravel ftc06–08, ftc06–09, and ftc06–12. *G*, ftc06–13, ftc06–14, and ftc06–15. *H*, Flowers surrounding the C1 calibration site.

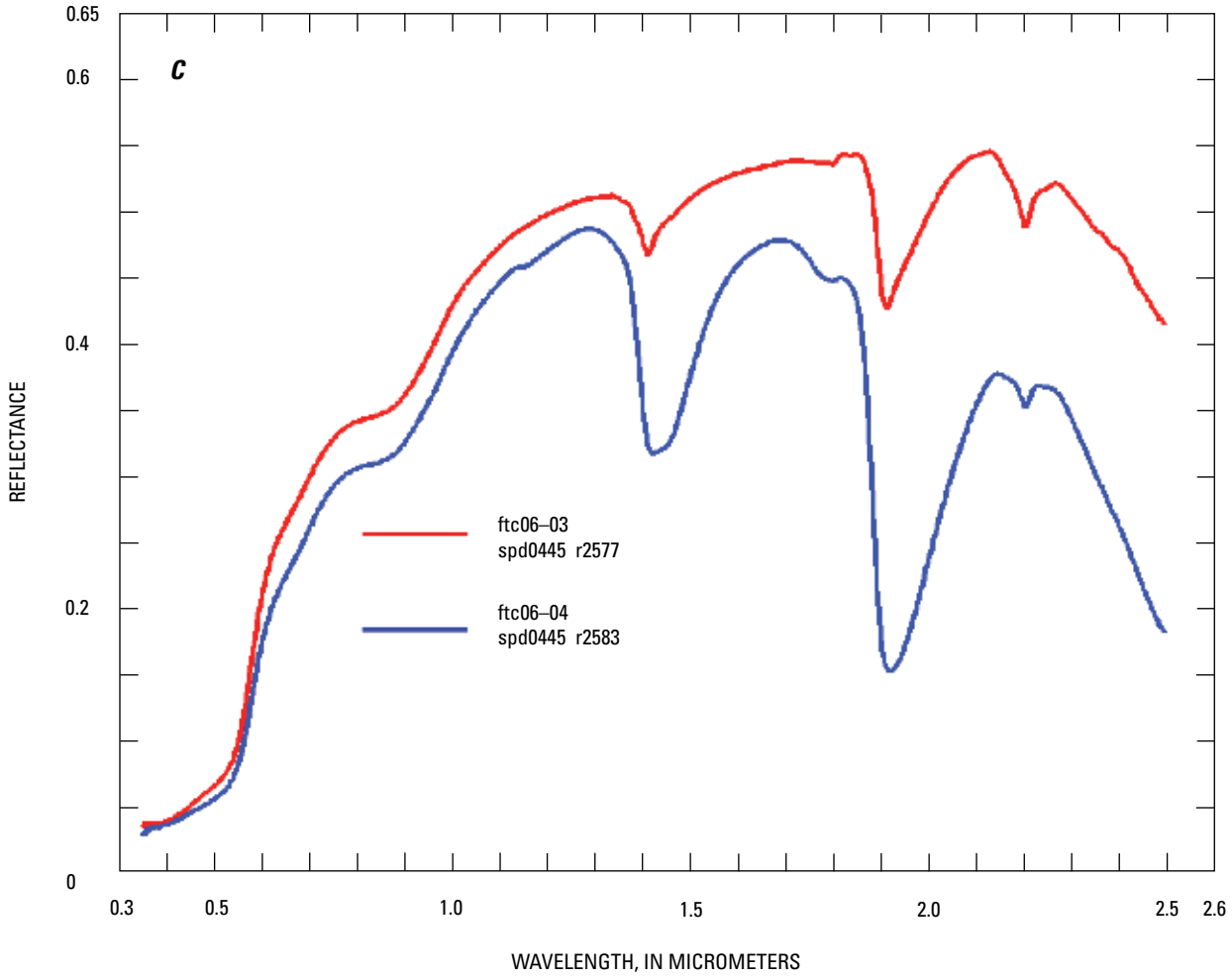

Note:
spd, spectral power distribution of the illuminant
r, reflectance of the object

Figure 4. Spectra obtained in the field for samples from Fort Cobb Reservoir watershed, southwestern Oklahoma. *A*, ftc06–01 and ftc06–02. *B*, ftc06–C1. *C*, ftc06–03 and ftc06–04. *D*, ftc06–05, ftc06–06, ftc06–10, and ftc06–11. *E*, ftc06–07 (high water content compared to ftc06–10 and ftc06–11. *F*, carbonate (dolomite) road gravel ftc06–08, ftc06–09, and ftc06–12. *G*, ftc06–13, ftc06–14, and ftc06–15. *H*, Flowers surrounding the C1 calibration site.

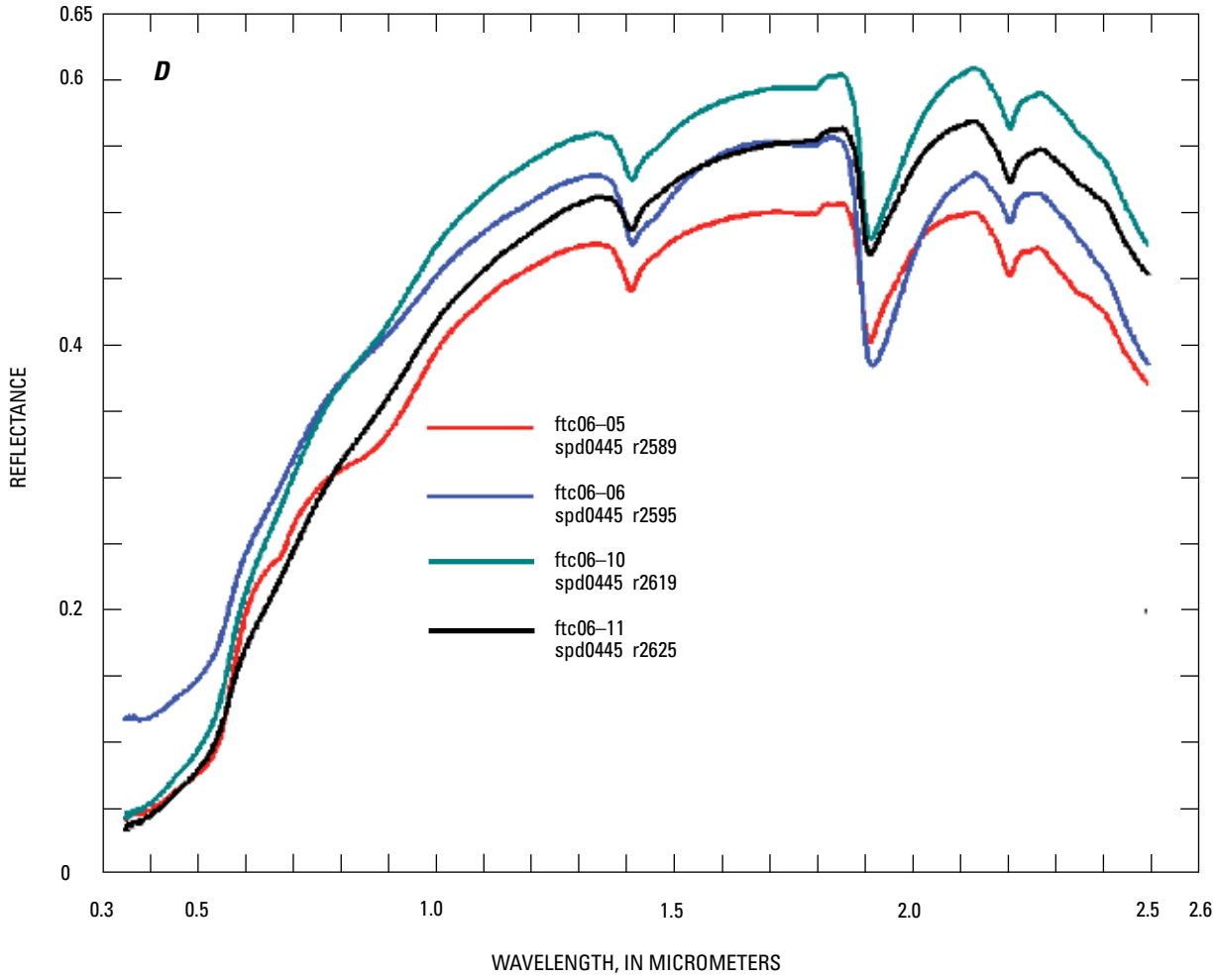

Note:
spd, spectral power distribution of the illuminant
r, reflectance of the object

Figure 4. Spectra obtained in the field for samples from Fort Cobb Reservoir watershed, southwestern Oklahoma. *A*, ftc06–01 and ftc06–02. *B*, ftc06–C1. *C*, ftc06–03 and ftc06–04. *D*, ftc06–05, ftc06–06, ftc06–10, and ftc06–11. *E*, ftc06–07 (high water content compared to ftc06–10 and ftc06–11. *F*, carbonate (dolomite) road gravel ftc06–08, ftc06–09, and ftc06–12. *G*, ftc06–13, ftc06–14, and ftc06–15. *H*, Flowers surrounding the C1 calibration site.

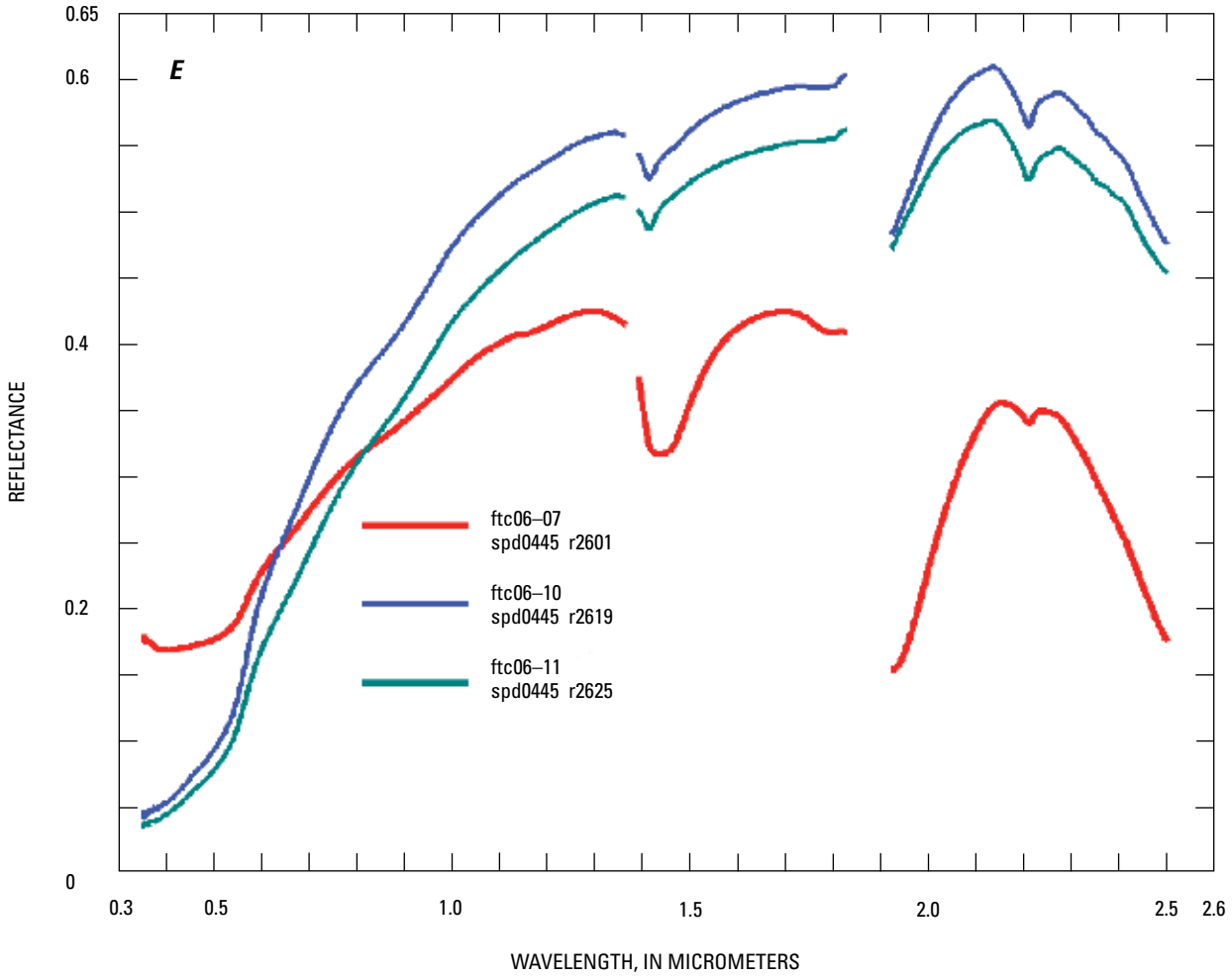

Note:
spd, spectral power distribution of the illuminant
r, reflectance of the object

Figure 4. Spectra obtained in the field for samples from Fort Cobb Reservoir watershed, southwestern Oklahoma. *A*, ftc06–01 and ftc06–02. *B*, ftc06–C1. *C*, ftc06–03 and ftc06–04. *D*, ftc06–05, ftc06–06, ftc06–10, and ftc06–11. *E*, ftc06–07 (high water content compared to ftc06–10 and ftc06–11. *F*, carbonate (dolomite) road gravel ftc06–08, ftc06–09, and ftc06–12. *G*, ftc06–13, ftc06–14, and ftc06–15. *H*, Flowers surrounding the C1 calibration site.

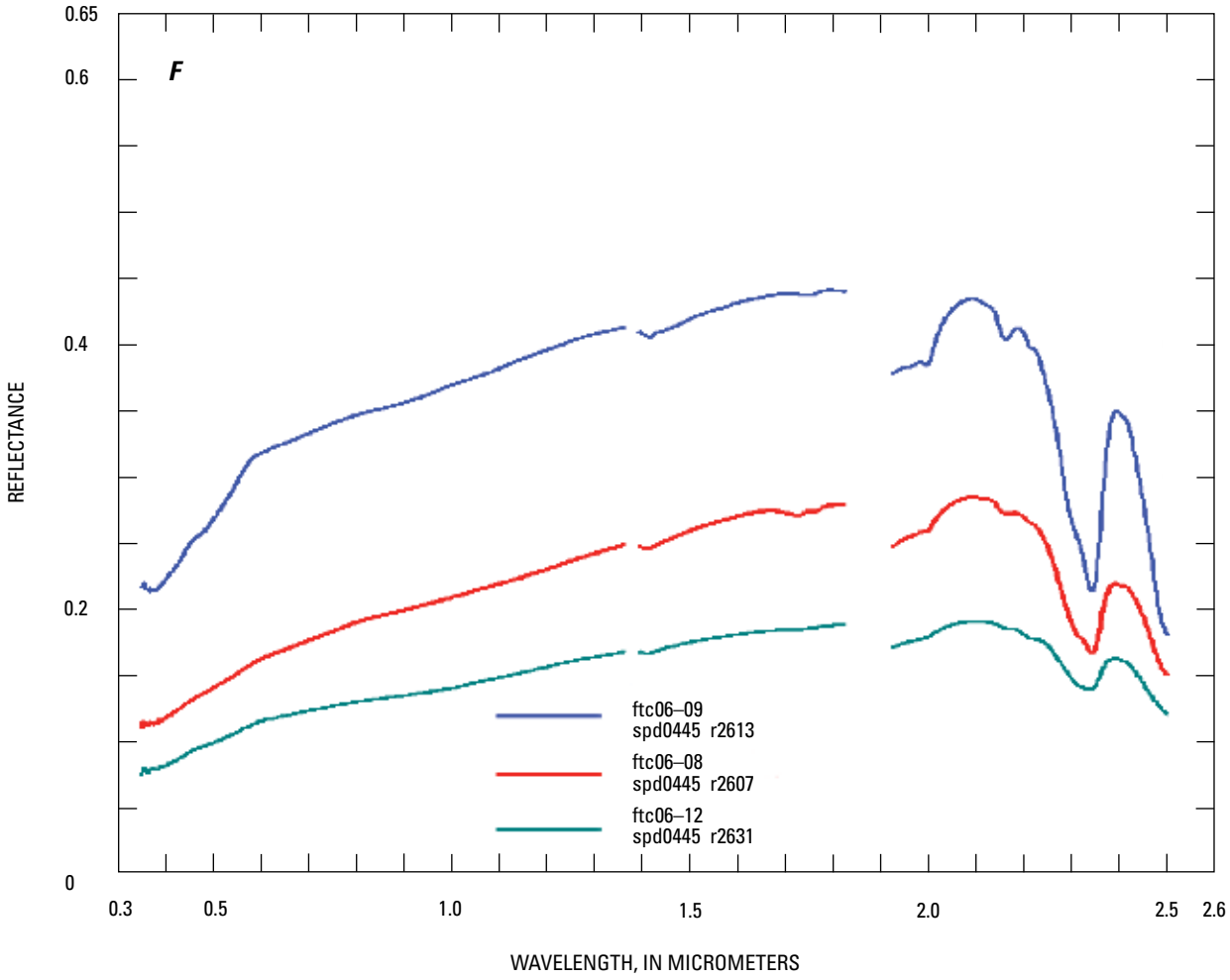

Note:
spd, spectral power distribution of the illuminant
r, reflectance of the object

Figure 4. Spectra obtained in the field for samples from Fort Cobb Reservoir watershed, southwestern Oklahoma. *A*, ftc06–01 and ftc06–02. *B*, ftc06–C1. *C*, ftc06–03 and ftc06–04. *D*, ftc06–05, ftc06–06, ftc06–10, and ftc06–11. *E*, ftc06–07 (high water content compared to ftc06–10 and ftc06–11. *F*, carbonate (dolomite) road gravel ftc06–08, ftc06–09, and ftc06–12. *G*, ftc06–13, ftc06–14, and ftc06–15. *H*, Flowers surrounding the C1 calibration site.

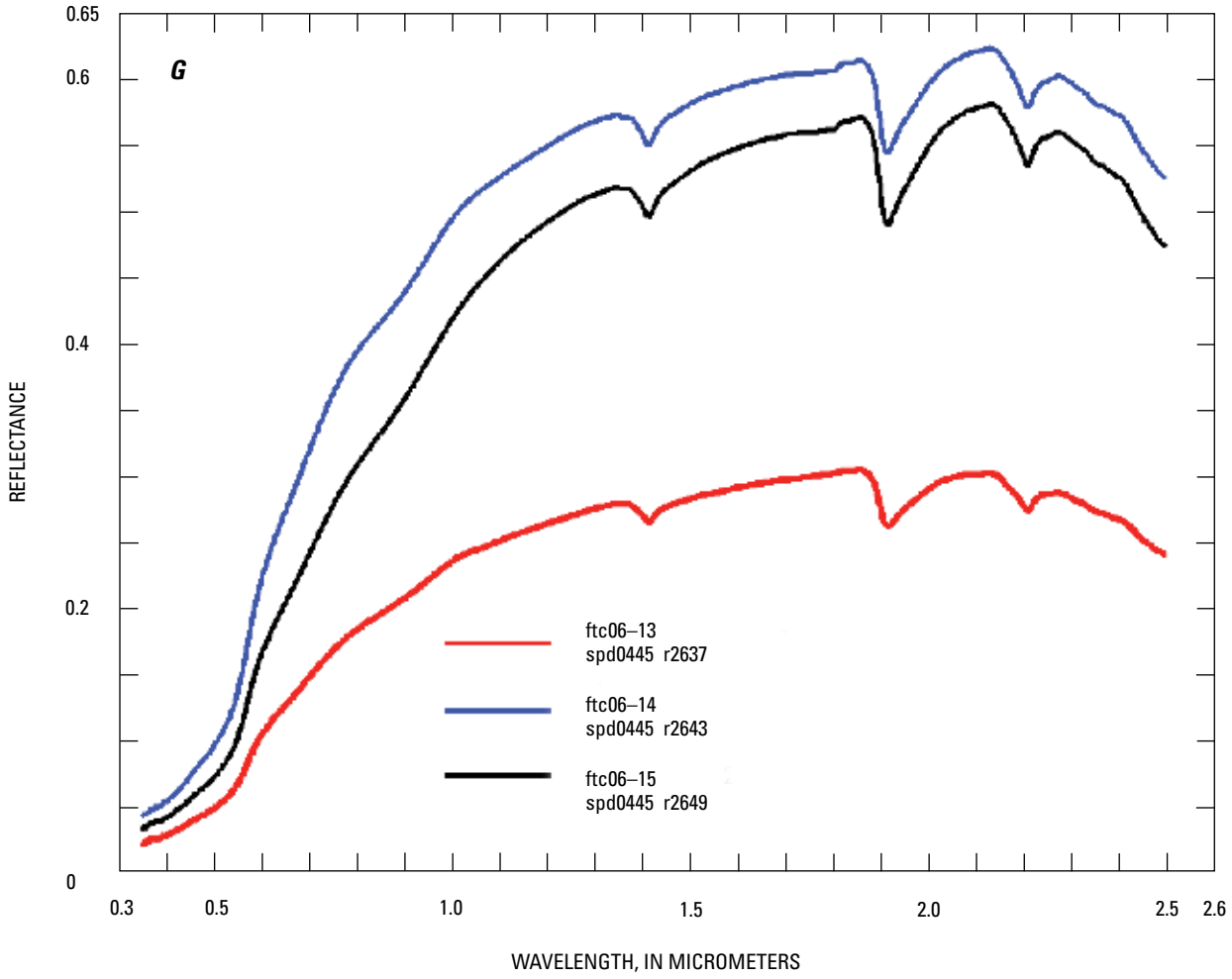

Note:
spd, spectral power distribution of the illuminant
r, reflectance of the object

Figure 4. Spectra obtained in the field for samples from Fort Cobb Reservoir watershed, southwestern Oklahoma. *A*, ftc06–01 and ftc06–02. *B*, ftc06–C1. *C*, ftc06–03 and ftc06–04. *D*, ftc06–05, ftc06–06, ftc06–10, and ftc06–11. *E*, ftc06–07 (high water content compared to ftc06–10 and ftc06–11. *F*, carbonate (dolomite) road gravel ftc06–08, ftc06–09, and ftc06–12. *G*, ftc06–13, ftc06–14, and ftc06–15. *H*, Flowers surrounding the C1 calibration site.

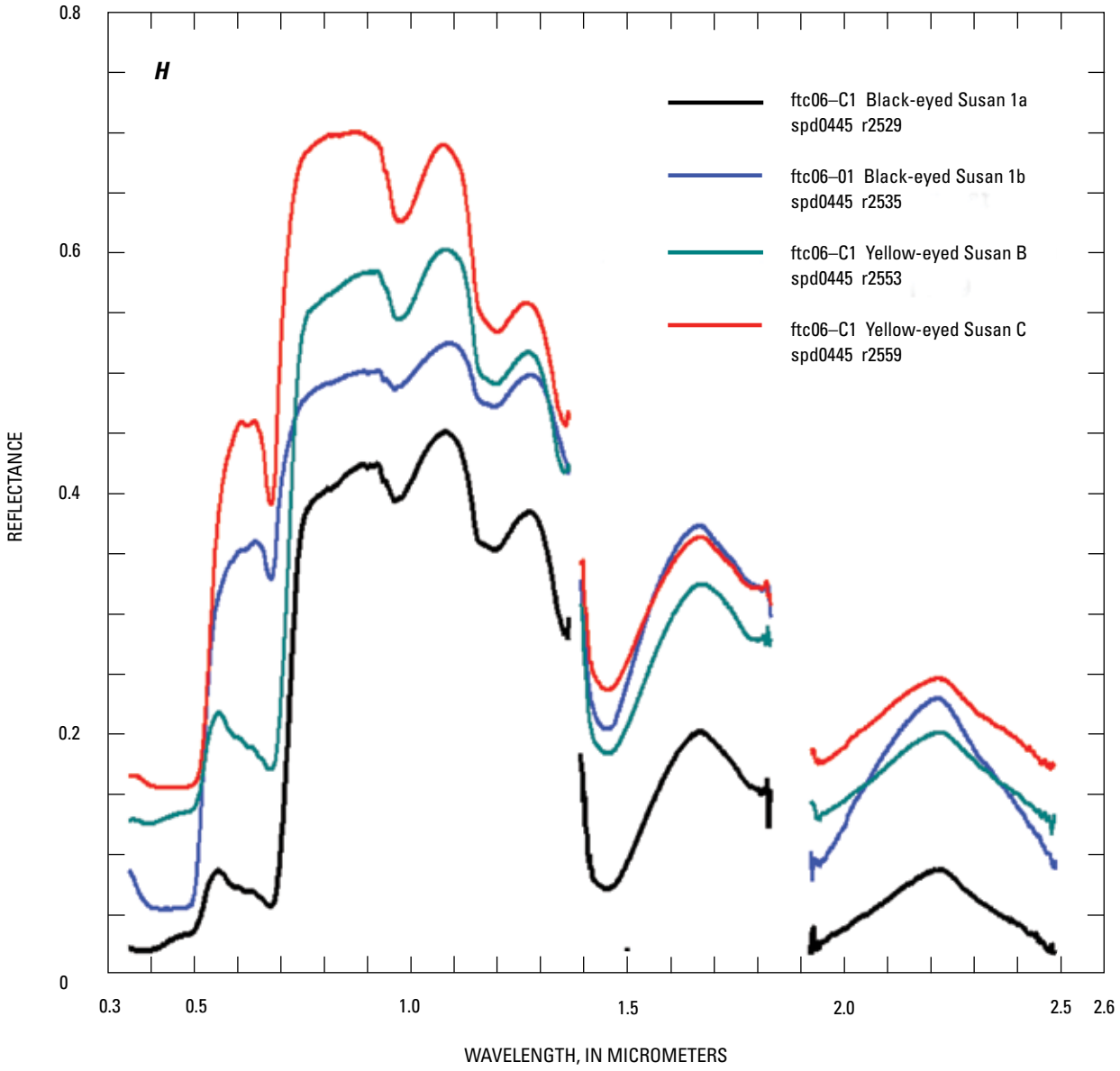

Note:
spd, spectral power distribution of the illuminant
r, reflectance of the object

Figure 4. Spectra obtained in the field for samples from Fort Cobb Reservoir watershed, southwestern Oklahoma. *A*, ftc06–01 and ftc06–02. *B*, ftc06–C1. *C*, ftc06–03 and ftc06–04. *D*, ftc06–05, ftc06–06, ftc06–10, and ftc06–11. *E*, ftc06–07 (high water content compared to ftc06–10 and ftc06–11. *F*, carbonate (dolomite) road gravel ftc06–08, ftc06–09, and ftc06–12. *G*, ftc06–13, ftc06–14, and ftc06–15. *H*, Flowers surrounding the C1 calibration site. The spectra of flowers were obtained to confirm that spectra extracted from the Hyperion data over the calibration site were free of spectral contamination from flowers.

was created that identified the offset and corrected the offset by extrapolating data on either side of identified offsets and deriving a correction to bring the spectra into alignment. Because of noise in the sensor, only about 90 percent of the offset could be corrected. This correction resulted in the ability to map strong absorption features in the visible part of the spectrum, but residual offsets affected weaker absorption bands. Therefore, line FCRW2 indicated reduced detections of iron oxides and vegetation, as shown in the maps. The offsets, however, did not affect the maps of chlorophyll in water.

Imaging Spectroscopy Mapping for Abundances of Chlorophyll, Iron Oxides, and Terrestrial Vegetation

Spectra of the samples of rocks and soils measured in the field (figs. 4*A*-4*G*) indicated that the steeply decreasing reflectance from about 1.5 microns toward shorter wavelengths (0.35-micron) is caused by hematite. Hematite reflectance also causes the weak absorptions near 0.9 and 0.7 microns and the inflection near 0.5 micron. The absorption near 1.9 microns is because of a combination of an O-H stretch plus the H-O-H bend in the water molecule, which indicates how much water is in the sample. The absorption near 1.4 microns is caused by the first overtone of the O-H stretch in either water molecules or hydroxyl ions. The absorption near 2.2 microns is because of a hydroxyl O-H stretch plus an aluminum-O-H bend in phyllosilicate minerals. Most of the absorption is caused by the clay mineral montmorillonite with contributions of kaolinite and muscovite/illite. The strength of the hematite 0.8-micron absorption, the 1.9-micron water absorption, and the 2.2-micron clay absorption for the field samples are listed in table 3. Spectra of flowers (ftc06-C1, fig. 4*H*) were obtained to confirm spectra extracted from the Hyperion data over calibration site C1 were free of spectral contamination from the flowers.

X-ray diffraction analysis of one sample, ftc06-02, indicated major quartz, weak feldspar (anorthite, albite), with minor muscovite, montmorillonite and kaolinite. X-ray diffraction did not detect any hematite, despite the strong red color of the sample. Reflectance spectroscopy has excellent sensitivity to hematite and clays and indicated that montmorillonite was higher in abundance than either kaolinite or muscovite in all the red soils and sandstones measured for this study. Near-infrared spectroscopy, which was used for this field work, is not sensitive to quartz and feldspar (mid-infrared spectroscopy has excellent sensitivity to these minerals) (Clark, 1999).

Once calibrated, the Hyperion data were analyzed with the U.S. Geological Survey Tetracorder algorithm (Clark and others, 2003a). This algorithm uses reference spectra (Clark and others, 2003b) to compare known spectral features to spectra in the imaging spectrometer data. The Hyperion data were analyzed by using 322 reference spectra of minerals, vegetation, water, manmade compounds and mixtures. The Tetracorder analysis produced three output images for each of the 322 reference spectra: (1) weighted absorption depth, (2) weighted correlation coefficient to the modified least squares fitting routine, and (3) weighted depth multiplied by correlation coefficients. The weighting used the normalized area of the spectral features from the reference spectra that was used for the fitting algorithm. The images shown on figures 5, 6, 7, 8*A*, and 8*B* are the weighted absorption depth multiplied by the correlation coefficient images. These images have the highest probability of correct identification (Clark and others, 2003a).

The two flight lines shown on figure 5 were separated in time by over one month, and no adjustments in level were made to any data. Calibration to reflectance compensates for the difference in sun angle and for the change in atmospheric absorption and scattering. In the overlay of these two lines, FCRW2 is shown on top, whereas in all other maps, FCRW1 is shown on top to allow the reader to compare the overlap region. Figure 5*A* shows a false-color composite of visible and near-infrared wavelengths. The images show cultivated fields surrounding the reservoir and the streams feeding into the reservoir. The colors show no obvious trend with distance from streams or the reservoir, with brighter green indicating

Table 3. Field-sample absorption feature strengths for the spectra images taken in the Fort Cobb watershed, southwestern Oklahoma, 2006.

Sample	Hematite 0.8-micron absorption	Water 1.9-micron absorption	Clay 2.2-micron absorption
ftc06-01	0.052	0.259	0.062
ftc06-02	0.072	0.310	0.062
ftc06-03	0.078	0.213	0.083
ftc06-04	0.092	0.641	0.053
ftc06-05	0.061	0.203	0.069
ftc06-06	0.009	0.300	0.054
ftc06-07	0.009	0.604	0.033
ftc06-10	0.015	0.205	0.058
ftc06-11	0.011	0.170	0.062
ftc06-13	0.011	0.140	0.068
ftc06-14	0.012	0.115	0.055
ftc06-15	0.015	0.145	0.061

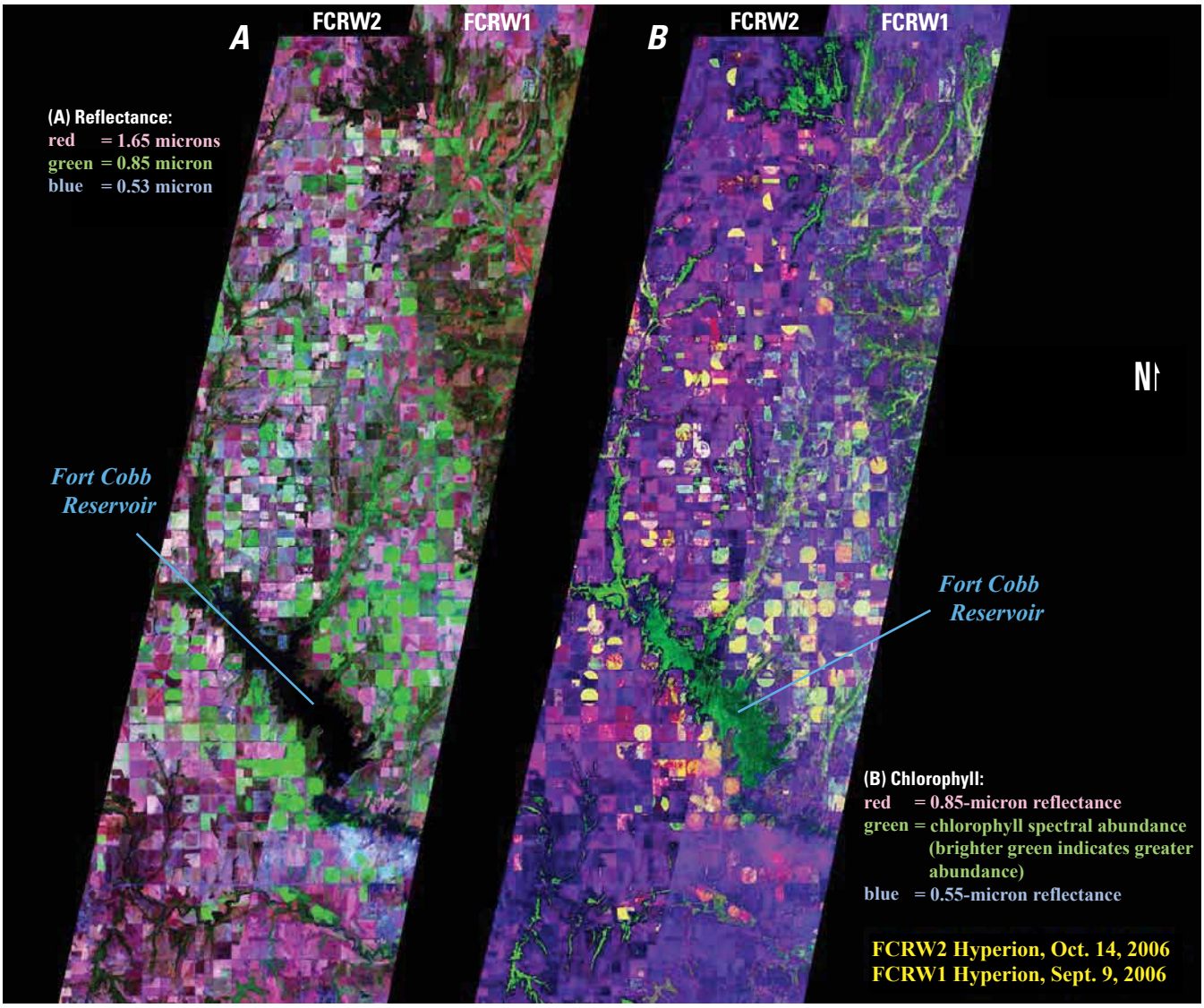

Figure 5. Hyperion imaging for the FCRW1 and FCRW2 flight lines for part of the Fort Cobb Reservoir watershed, southwestern Oklahoma, 2006. *A*, False color composite. *B*, False color composite with the green channel replaced with map of the chlorophyll reflectance peak (brighter color correlates to greater abundance).

Figure 6. Tetracorder-derived mineral map (Clark and others, 2003a) for absorption features occurring in the visible portion of the spectrum, including those caused by iron oxides and vegetation from part of the Fort Cobb Reservoir watershed, southwestern Oklahoma, 2006.

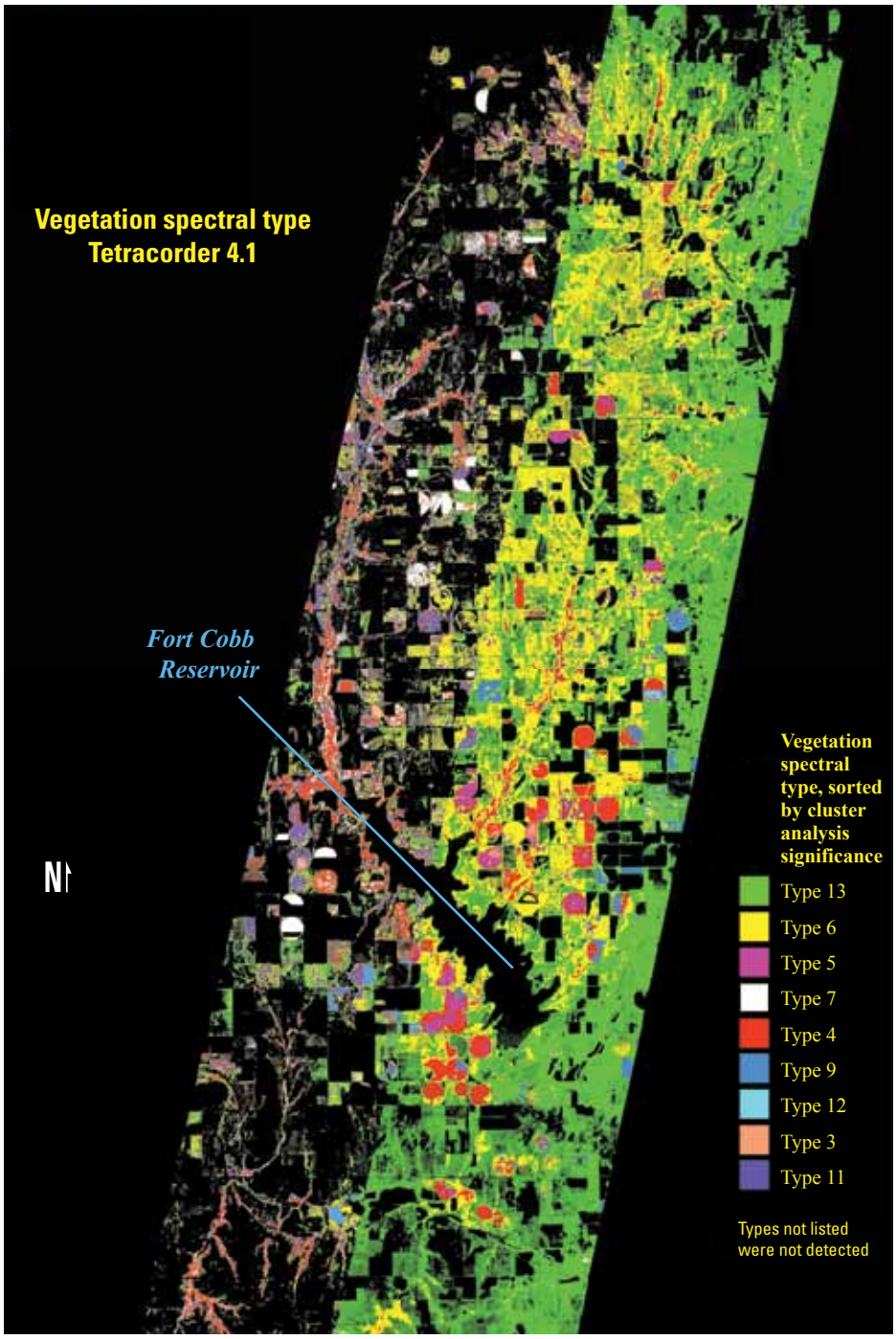

Figure 7. Vegetation spectral type using spectral feature matching methods of Tetracorder (Clark and others, 2003a) in part of the Fort Cobb Reservoir watershed, southwestern Oklahoma, 2006.

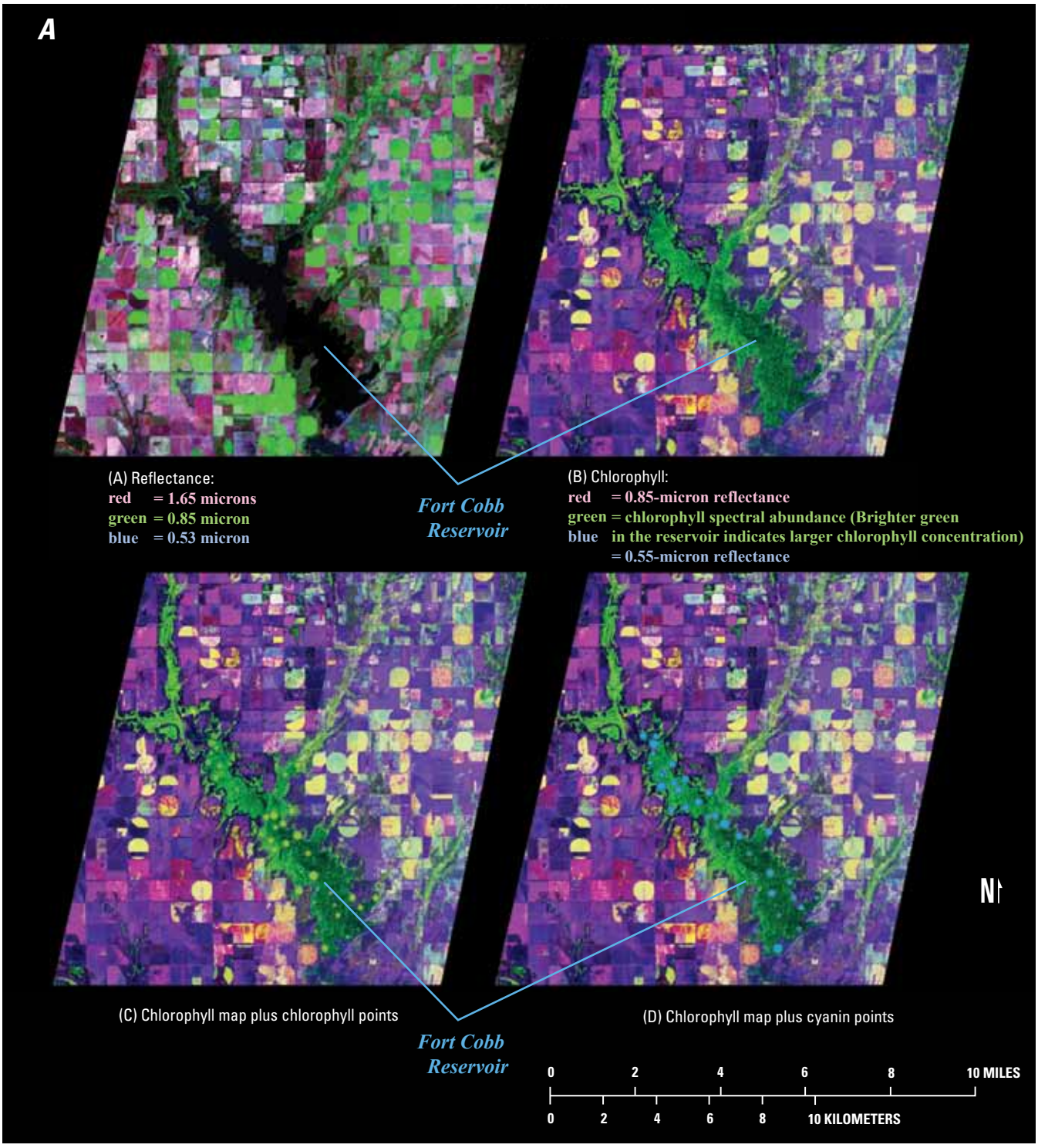

Figure 8. *A*, The Hyperion maps from figure 5 (with line FCRW1 on top) are shown with reservoir sampling and laboratory-derived chlorophyll and photocyanin concentrations (from chapter 8 of this report), Fort Cobb Reservoir, southwestern Oklahoma, 2006. Larger point sizes in panels C (green circles in the reservoir) and D (blue circles in the reservoir) indicate greater abundances.

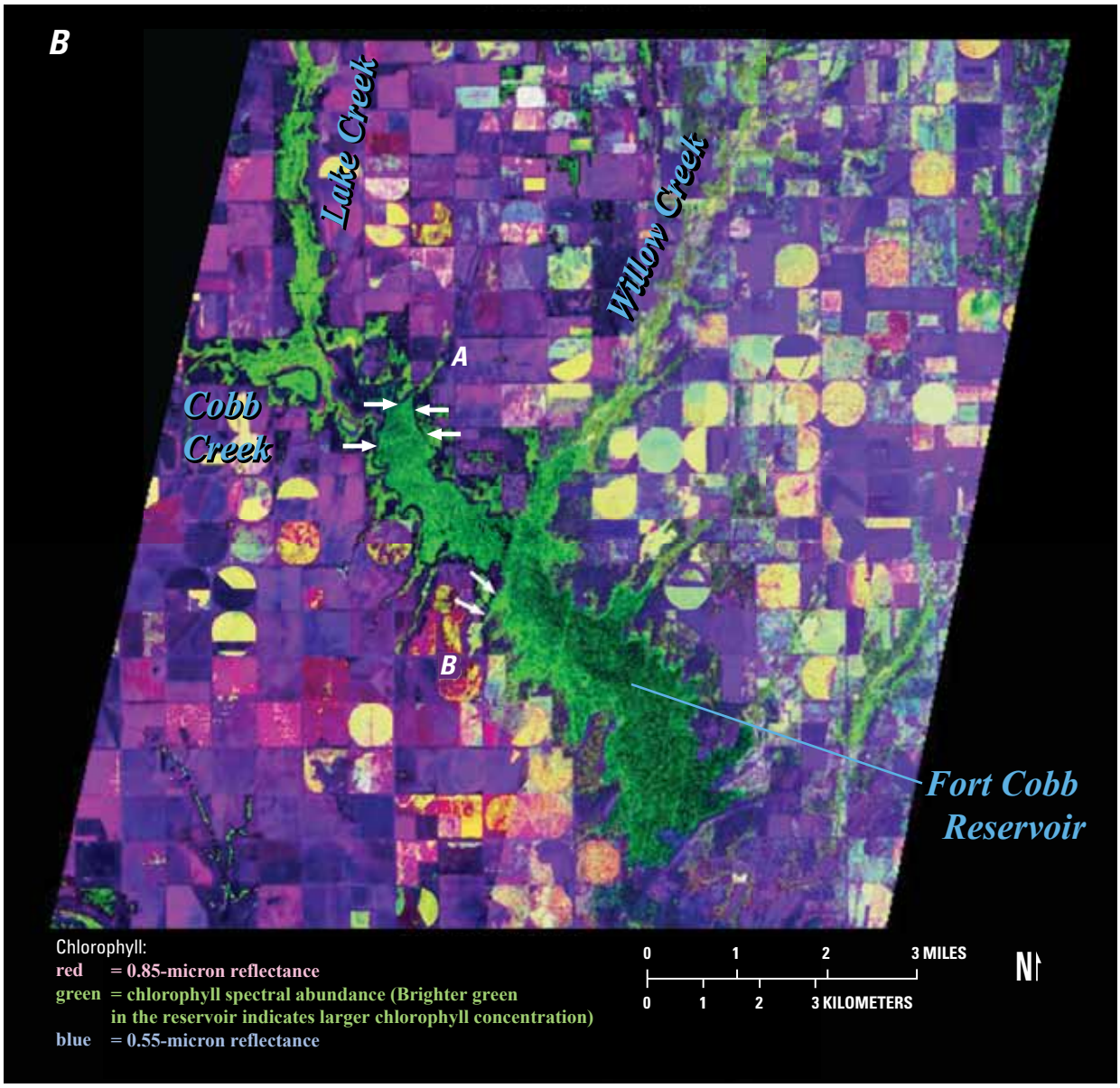

Figure 8. *B*, Same as figure 8*A*, panel B, enlarged with labels. Locations A and B show high chlorophyll in water (arrows) emanating from streams draining from cultivated fields.

higher chlorophyll content. Chlorophyll spectral abundance is shown in figure 5*B*. The chlorophyll in the Fort Cobb Reservoir indicated that (1) each of the major streams feeding into the reservoir indicated a trail of higher chlorophyll content; (2) higher chlorophyll concentrations tended to occur along the southwest side of the reservoir, whether the higher chlorophyll contents are because of nutrients entering that side of the reservoir or if currents are bringing nutrients to that side is not clear, but some small drainages appeared to be sources for at least some of the chlorophyll; (3) a continuous path of chlorophyll from Willow Creek entered the reservoir (fig. 1), and may be at least a partial explanation for the high chlorophyll in the reservoir; (4) similarly, Lake Creek and Cobb Creek appeared to be sources of high chlorophyll; and (5) the small creek (labeled A in figure 8*B*) between Lake and Willow Creeks may be a similarly high chlorophyll source. This creek drained directly from cultivated fields, whereas the major creeks (Willow, Lake, and Cobb) had more natural ecosystems that acted as a buffer for runoff from farm fields.

Iron oxide spectral abundance is shown in figure 6. The FCRW2 image results were increased by about 10 percent to match the FCRW1 results for the iron oxides. The lower response of FCRW2 was because of residual offsets in the data. The bare farm fields indicated the strongest signatures. Iron oxide content indicated little regional trend, except for a tendency for stronger spectral signatures to the north. This strong spectral signature corresponded to the reddish coloration of the soils during field calibration efforts. Fields to the north tended to indicate a stronger red color from visual reconnaissance during our calibration and sampling trip, and in measured hematite absorption strengths in field samples (for example, samples ftc06-11 through fct01-15 in table 3), but not universally (for example, sample ftc06-10). The Hyperion data indicate large heterogeneity in adjacent fields (fig. 6). Local crops and/or farming practices might preferentially leach iron oxide from the soil, thus explaining why some fields indicated different iron oxide spectral strengths compared to an adjacent field.

The terrestrial vegetation spectral map, figure 7, also indicated no obvious trend in relation to chlorophyll abundance in the reservoir. Confounding attempts to determine a relation between these variables is the fact that line FCRW2 was obtained nearly a month after line FCRW1 and vegetation was senescing with the start of autumn. The feature match used spectra from the U.S. Geological Survey spectral library (Clark and others, 2003b) and do not identify species. The same colors indicate the same spectral match to the reference spectra and may indicate the same species in the scene but not to the reference material. This is because vegetation spectra change with time, especially during autumn senescence. To identify species, reference spectra of each species in the scene are required at the time of the flight. This map indicates major changes with the onset of autumn, but does not show any obvious relationship to water-quality issues with the reservoir.

Attempts were made to map clay abundance using the 2.2-micron features, but the Hyperion sensor had insufficient signal-to-noise ratio at those wavelengths. Also, the sensor had increased and varied ringing in the data beyond 2 microns, making only the strongest absorptions detectable. Spectra of the field samples also indicated no obvious trends. With the entire region consisting of similar geologic units, mineral abundances were mostly constant.

The chlorophyll abundance map from Hyperion was combined with chlorophyll and photocyanin data from field sampling (from Fairchild and Allert, 2010, chapter 8 of this report) in figure 8*A* to illustrate the similarities and differences found by each method. The chlorophyll map, enlarged 2x, with labels is shown in figure 8*B*. Example spectra that indicated the chlorophyll reflection peak in the visible part of the spectrum are shown in figure 9. Water sampling and laboratory analysis produces a more accurate picture for a small number of points. Remote sensing data provides continuous spatial sampling but the results in this case are qualitative. The chlorophyll map from Hyperion data indicates multiple sources from streams entering the reservoir where the chlorophyll concentration in the reservoir was high. Lake, Willow, and Cobb Creeks contribute chlorophyll to the reservoir, the smaller creeks also contribute, and perhaps in greater proportions, relative to the size of those small creeks. For example, for the stream labeled A in figure 8*B* between Lake and Willow Creeks that was draining into Fort Cobb Reservoir from the north-to-northwest, a substantial plume appeared in the reservoir at the mouth of this stream (arrows in figure 8*B*). Directly on the opposite shore from Willow Creek was another smaller drainage, labeled B in figure 8*B*, where there was another substantial chlorophyll plume near the shore of the reservoir. These drainages drained directly from farm fields, whereas the major creeks (Lake, Willow, and Cobb Creeks) include natural aquatic and terrestrial ecosystems that should help to buffer pollution.

In general, natural ecosystems filter pollution, and should help provide a buffer from fertilizer and pesticides that enter stream water and lakes. Remote sensing data indicated that many farm fields in the Fort Cobb watershed drained directly into streams and lakes with little natural intervening ecosystems to buffer runoff. One solution to the future health of the reservoir may be to increase the number and size of natural areas (such as riparian buffer strips) around all drainages to the reservoir.

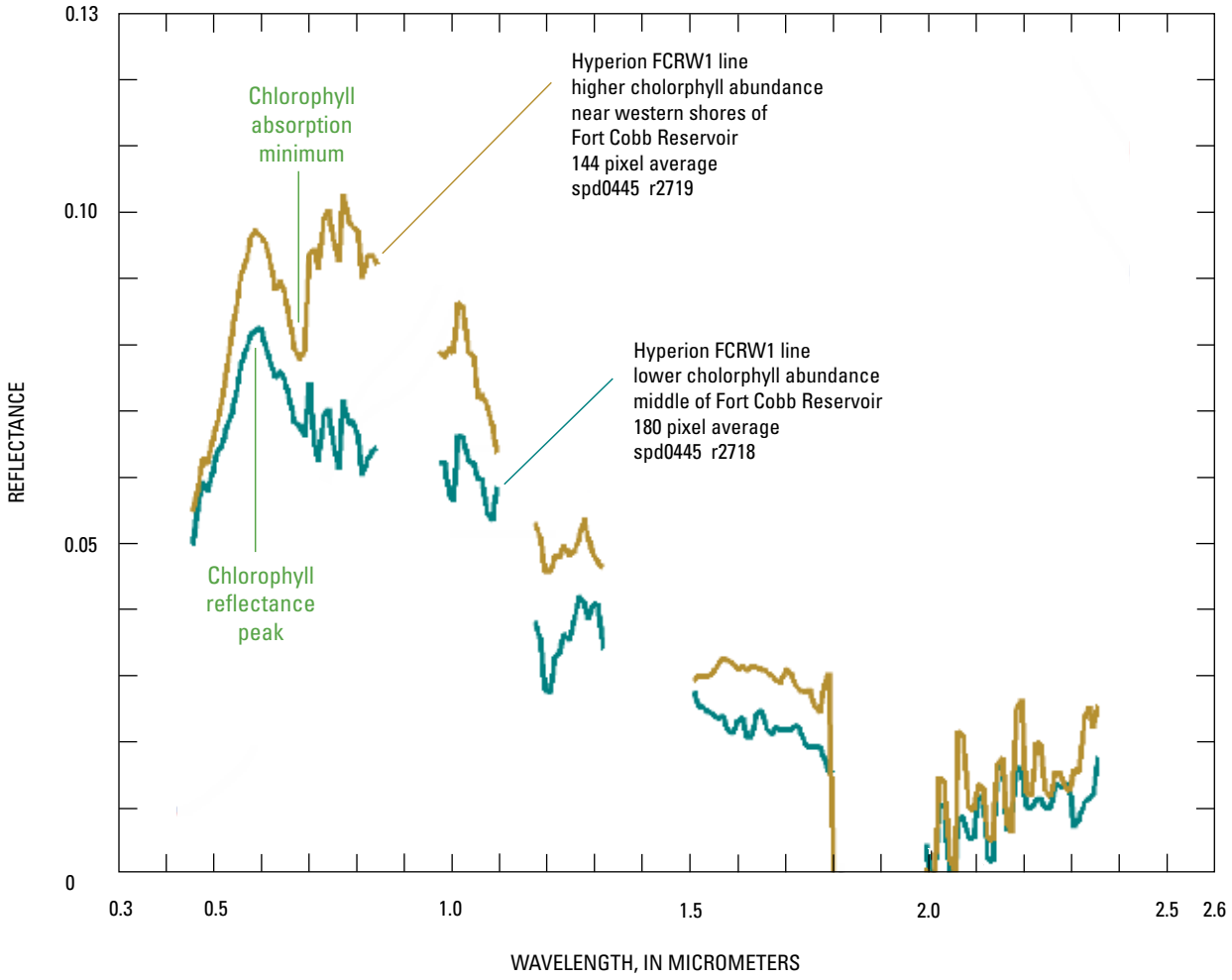

Note:
spd, spectral power distribution of the illuminant
r, reflectance of the object

Figure 9. Representative Hyperion spectra of chlorophyll-containing water of the Fort Cobb Reservoir, southwestern Oklahoma, 2006.

Summary and Conclusions

Imaging spectroscopy remote sensing was used to estimate concentrations of selected compounds in the Fort Cobb Reservoir watershed of southwest Oklahoma. The Hyperion sensor measures spectra from the ultraviolet (0.35 microns) to the near-infrared (2.5 microns). The signal-to-noise ratio was not as high as other sensors, but the signal-to-noise ratio is adequate for compounds with major absorption bands in those spectra. Estimated abundance of chlorophyll in water, iron oxides, and terrestrial vegetation were successfully mapped. A portable field spectrometer was used in September 2006 to measure characteristic spectral reflectance properties of soils in the watershed. Data from the field spectrometer were used to calibrate the Hyperion data, removing atmospheric scattering and absorptions and removing the solar spectrum, resulting in calibrated reflectance spectra on a 30-meter spatial grid throughout the imaged area. The spectra were then analyzed to search for compounds in each spectrum and maps of various compounds constructed. Different vegetation types also were distinguished but specific vegetation species were not determined.

Using imaging spectroscopy remote sensing, relative concentrations of chlorophyll in the Fort Cobb Reservoir could be seen. Some areas with greater chlorophyll concentrations appeared where streams flowed into the reservoir. Areas where some small creeks drained directly from cultivated fields coincided with plumes of relatively large chlorophyll concentrations in the reservoir, which may be related to natural ecosystems buffering fertilizer runoff from cultivated fields near the larger creeks. If natural ecosystems reduce runoff, then increased areas of natural ecosystems to create a buffer zone between cultivated fields and streams, lakes and reservoirs may improve water quality of the Fort Cobb and other reservoirs and lakes in the region. Further study would be needed to determine how large such natural areas would need to be for the ability to buffer runoff from cultivated fields.

Iron oxides occurred in greater abundance toward the northern region in the images, but throughout the study region, adjacent fields had differing iron oxide absorption strengths. These differing absorption strengths may indicate different farming practices in each that field leached the iron oxides in different amounts. Other compounds also may be leached in these different fields, but such determinations were beyond the scope of this study. However, the varied iron oxide abundances seen in the mineral maps could provide a starting point for future studies of soil chemistry.

The terrestrial vegetation spectral map indicated no obvious trend in relation to chlorophyll abundance in the reservoir. Confounding determination of such a relation is the fact that line FCRW2 was obtained nearly a month after line FCRW1 and vegetation was senescing with the start of autumn.

References Cited

Clark, R.N., 1999, Spectroscopy of rocks and minerals, and principles of spectroscopy, chapter 1 *in* A.N. Rencz, ed., Manual of remote sensing—Remote sensing for the earth sciences: New York, John Wiley and Sons, p. 3-58.

Clark, R.N., Swayze, G.A., Livo, K.E., Kokaly, R.F., King, T.V.V., Dalton, J.B., Vance, J.S., Rockwell, B.W., Hoefen, Todd, and McDougal, R.R., 2002, Surface reflectance calibration of terrestrial imaging spectroscopy data—A tutorial using AVIRIS, *in* Green, R.O., ed., Proceedings of the 10th Airborne Earth Science Workshop, NASA Jet Propulsion Laboratory publication 02-1, 2002, available online at http://speclab.cr.usgs.gov/PAPERS.calibration.tutorial/ (accessed December 15, 2009).

Clark, R.N., Swayze, G.A., Livo, K.E., Kokaly, R.F., Sutley, S.J., Dalton, J.B., McDougal, R.R., and Gent, C.A., 2003a, Imaging spectroscopy—Earth and planetary remote sensing with the USGS Tetracorder and expert systems: Journal of Geophysical Research, vol. 108, no. E12, 5131, doi:10.1029/2002JE001847, pages 5-1 to 5-44, available online at http://speclab.cr.usgs.gov/PAPERS/tetracorder (accessed June 1, 2008).

Clark, R.N., Swayze, G.A., Wise, Richard, Livo, K.E., Hoefen, T.M., Kokaly, R.F., and Sutley, S.J., 2003b, USGS Digital Spectral Library splib05a: U.S. Geological Survey Open File Report 03-395, available online at http://speclab.cr.usgs.gov/spectral-lib.html (accessed December 15, 2010).

Pearlman, J., Carman, S., Segal, C., Jarecke, P., Clancy, P., and Browne, W., 2001, Overview of the Hyperion Imaging Spectrometer for the NASA EO-1 mission *in* Geoscience and Remote Sensing Symposium, 2001. IGARSS ‘01: IEEE 2001 International, v. 7, p. 3036-3038.

Runkle, D.L., Rea, Alan, and Becker, M.F., 1997, Digital data sets that describe aquifer characteristics of the Rush Springs aquifer in western Oklahoma: U.S. Geological Survey Open-File Report 96-453.

Suneson, N.H., and Johnson, M.F., 1996, Geology of Red Rock Canyon State Park: Oklahoma Geological Survey, Oklahoma Geology Notes, v. 56, no. 3, p. 88-105.